Title: Coseismic deformation and source modeling of the May 2012 Emilia (Northern Italy) earthquakes

Authors: Giuseppe Pezzo(1), John Peter Merryman Boncori(1), Cristiano Tolomei(1), Stefano Salvi(1), Simone Atzori(1), Andrea Antonioli(1), Elisa Trasatti(1), Fabrizio Novali(2), Enrico Serpelloni(3), Laura Candela(4), Roberta Giuliani(5)

(1): Istituto Nazionale di Geofisica e Vulcanologia, Centro Nazionale Terremoti, via di Vigna Murata 605, 00143 Roma, Italy

(2): Tele-Rilevamento Europa - T.R.E. srl, Via Vittoria Colonna 7, 20149 Milano, Italy.

(3): Istituto Nazionale di Geofisica e Vulcanologia – Centro Nazionale Terremoti, via D. Creti, 12, 40128 Bologna, Italy

(4): Agenzia Spaziale Italiana, Unità Osservazione della Terra, Viale Liegi 26, 00198, Roma, Italy

(5): Dipartimento della Protezione Civile, Ufficio Rischio Sismico, Via Vitorchiano 4, 00189 Roma, Italy

Running Title: Coseismic dislocation modeling of Emilia earthquakes

Supplemental material: a single .doc document containing additional figures and tables.

Corresponding author:

Giuseppe Pezzo

Istituto Nazionale di Geofisica e Vulcanologia,

Via di Vigna Murata, 605, 00143 Roma, Italy;

phone: +390651860643;

email: giuseppe.pezzo@ingv.it

Keywords: Satellite geodesy; Radar interferometry; Coseismic ground displacement; Seismicity and tectonics;

1. Introduction

On May 20th, 2012, an M_L 5.9 earthquake (Table 1) occurred near the town of Finale Emilia, in the Central Po Plain, Northern Italy (Figure 1). The mainshock caused 7 casualties and the collapse of several historical buildings and industrial sheds. The earthquake sequence continued with diminishing aftershock magnitudes until May 29th, when an M_L 5.8 earthquake occurred near the town of Mirandola, ~12 km WSW of the mainshock (Scognamiglio *et al.*, 2012). This second mainshock started a new aftershock sequence in this area, and increased structural damage and collapses, causing 19 more casualties and increasing to 15.000 the number of evacuees.

Shortly after the first mainshock, the Department of Civil Protection (DPC) activated the Italian Space Agency (ASI), which provided post-seismic SAR Interferometry data coverage with all 4 COSMO-SkyMed SAR satellites. Within the next two weeks, several SAR Interferometry (InSAR) image pairs were processed by the INGV-SIGRIS system (Salvi *et al.*, 2012), to generate displacement maps and preliminary source models for the emergency management. These results included continuous GPS site displacement data, from private and public sources, located in and around the epicentral area.

In this paper we present the results of the geodetic data modeling, identifying two main fault planes for the Emilia seismic sequence and computing the corresponding slip distributions. We discuss the implication of this seismic sequence on the activity of the frontal part of the Northern Apennine accretionary wedge by comparing the co-seismic data with the long term (geological) and present day (GPS) velocity fields.

2. Tectonic framework

The Emilia region is located in the Po Plain, which represents the E-W continental collisional boundary between the subducting Adria plate to the North, and the overriding Northern Apennine block to the South (Picotti & Pazzaglia, 2008). The related thrust belt-foredeep system developed as the result of the late-Oligocene to present, NNE rollback of the W-oriented subducting slab (e.g. Faccenna *et al*. 2003 Bennet *et al.*, 2012).

The 2012 seismic sequence occurred in the Central Po Plain tectonic domain, characterized, below the Plio-Quaternary sedimentary cover, by arcuate thrust systems and related growth folds (Pieri and Groppi 1981; Pieri, 1983; Consiglio Nazionale delle Ricerche, 1992). These structures are well imaged by several seismic sections acquired by the petroleum industry in the last 30 years (Boccaletti & Martelli, 2004); these thrusts are considered blind, since no fault traces can be seen at the surface (Burrato *et al.*, 2003).

The activity of the thrust-fold system has been debated for many years. Some authors, based on field studies and seismic reflection lines, maintain the hypothesis that following a major geodynamic change, thrusting and related folding between the northern front of the Apennine and the Po Plain ceased in Early Pleistocene time (Argnani *et al*. 1997; Bertotti *et al*. 1997; Di Bucci and Mazzoli 2002; Argnani *et al.*, 2003). Other authors, based on geomorphological analysis, subsurface geology, seismicity and present day stress field, suggest that the tectonic activity of the frontal part of the Northern Apennine accretionary wedge is still going on (Meletti *et al*. 2000; Valensise and Pantosti, 2001; Boccaletti *et al*., 2004). In particular, Scrocca *et al*. (2007) and Burrato *et al.* (2003) suggest that this activity is mainly going on along the external thrust fronts below the Po plain. Active thrusting is also in agreement with recent horizontal GPS measurements (Serpelloni *et al.*, 2006; Devoti *et al.*, 2011) which suggest ~1 mm/yr of shortening accommodated

in this area. Such low deformation rates are in agreement with the low historical seismicity levels of the area. In fact, since at least the year 1000 A.D., this area has never experienced earthquakes of magnitude larger than Mw ~4.7 (1574 Finale Emilia earthquake, Rovida *et al.*, 2011), Larger magnitude earthquakes occurred West and East of the 2012 epicentral area, the most significant one being the 1570, Mw ~5.4, Ferrara earthquake (Rovida *et al.*, 2011).

The sources of such historical events (the Mirandola and Ferrara thrusts) were defined based on seismic reflection profiles and geomorphological studies (DISS Working Group, 2010; Bigi *et al.*, 1983; Basili *et al.*, 2008), their location roughly corresponding to the area of the 2012 sequence (Figure 1). In particular, Burrato *et al.* (2003) describe active fold growth in this area, observing the northward migration of the Po river and other smaller watercourses during the Upper Quaternary. The short-term co-seismic deformation observed during the seismic sequence may provide the opportunity to harmonize all geological long-term observations with the present day rates.

The 2012 earthquakes have actually confirmed the present activity of the external thrust belt (at least in the Central Po plain): the main focal solutions (Figure 1) show WNW to E-W nodal planes and a ~N-S compressional kinematics (Malagnini *et al.*, 2012), in agreement with the seismotectonic setting (Boccaletti *et al.*, 2010).

3. Geodetic Data

Our geodetic data consist of COSMO-SkyMed (hereinafter CSK) and Radarsat-1 InSAR data and GPS site displacements.

CSK is an Italian constellation of four satellites with a 16 day repeat cycle, launched between 2007 and 2010, each carrying the same X-band SAR instrument. The current orbital configuration allows InSAR pairs with temporal baselines of 1, 3, 4 and 8 days respectively to be formed within each

repeat cycle. For the current study two Strip-Map HIMAGE pairs were used (40 x 40 km swath, 3 x 3 m resolution on ground), acquired with beams H4-03 and H4-04. The Radarsat-1 satellite is a joint Canadian Space Agency (CSA) and NASA project. Launched in 1995, it operates in a 24-day repeat cycle, carrying a C-band SAR. For the current study a Standard Beam (S3) Strip-Map image pair was used (100 x 100 km swath, 5 x 20 m resolution on ground).

All interferograms were generated at a 90 m posting, using the SRTM 3 arc-sec DEM to remove the contribution of topography (Farr *et al.*, 2007), and a set of tie-points, from highly coherent regions outside the main displacement patterns, was used to estimate and remove the contribution of orbital uncertainties.

The first CSK interferogram, obtained from two descending acquisitions on May 19th and May 23rd (CSK1, Table 2), captures the easternmost part of the coseismic ground displacement of the first earthquake (Figures 2, S1A SUPPLEMENT and 3A SUPPLEMENT). In this area the maximum displacement is ~15 cm towards the satellite, with an increasing displacement expected beyond the western border of the image (Figure S1A SUPPLEMENT, 3A SUPPLEMENT). A second CSK interferogram from a different descending orbit, was calculated with the May 27th and June 4th pair (CSK2, Table 2), and yielded a well centered picture of the displacement field of the May 29th M_L 5.8 event, and of some other M_L >5 aftershocks (Table 1, Figures S1B SUPPLEMENT and 3G). A third displacement map was generated from a Radarsat-1 pair (RSAT, Table 2), spanning the whole seismic activity from May 12th to June 5th; this interferogram (Figure S1C SUPPLEMENT and 4A), shows the cumulated displacement field induced by all the events of Table 1, where the two main lobes are evidently due to the May 20th and May 29th events.

To obtain a full displacement field of the May 20th earthquake we subtracted the CSK2 displacement map from the Radarsat one. The differential displacement map (Figure 3D and 4B) represents the cumulated deformation from May 12th to May 27th, and from June 4th to June 5th (Figure 2). We

calculate (Figure S2 SUPPLEMENT) that the spatially correlated displacement error introduced by differencing these maps with only slightly different LoS vectors (Table 2), lies below ±3 mm for most areas, reaching a maximum of 8 mm close to the May 29th epicenter. These values are below the variance of differential turbulent tropospheric delays, in the order of 1.4 cm.

Coseismic displacements for the 20th and 29th May events were also derived from GPS data (Serpelloni, *et al.*, 2012). Most of the GPS site displacements were obtained for the far field, while only 3 were available for the epicentral area (Figure 3),

4. Data modeling

The seismic sources of the May 20th and May 29th events were modeled by inverting the abovementioned InSAR and GPS data, adopting the analytic solutions for the dislocation in an elastic half-space (Okada, 1985). InSAR data were first resampled to lower the computational load, using a regular sampling on a 400-m mesh grid (see Atzori and Antonioli, 2011). We then inverted the data with a two-step approach, consisting of a non-linear inversion based on the Levemberg-Marquardt algorithm (Levemberg, 1944; Marquardt, 1963) to study the source geometry with uniform slip, followed by a damped linear inversion to get the slip distribution (see Atzori *et al.*, 2009).

Since the InSAR displacement fields are nearly symmetrical with respect to an E-W axis, they could in principle be fit equally well by either North or South dipping dislocations. However, since the aftershock distribution (Marzorati *et al.*, 2012; http://iside.rm.ingv.it) and the geological constraints clearly indicate S-dipping fault planes, we discarded the possibility of N-dipping faults (Figure S3 SUPPLEMENT).

The best fit fault parameters resulting from the non-linear inversion are shown in Tables S1 SUPPLEMENT and S2 SUPPLEMENT, for the May 20th and May 29th earthquakes, respectively. To estimate the parameter standard deviations and trade-offs (Figure S4 SUPPLEMENT and S5 SUPPLEMENT), we ran 150 different non linear inversion restarts.

As mentioned before, the location and geometry of the main buried thrust faults of this area (the Ferrara and Mirandola thrusts) are well known from geological studies (Improta, L. Manuscript in preparation, 2012; Boccaletti *et al.*, 2010; Picotti and Pazzaglia, 2008; Bigi *et al.*, 1983). In Tables S1 SUPPLEMENT and S2 SUPPLEMENT we compare the Ferrara and Mirandola (geological) fault parameters with those resulting from the non linear inversion, together with source parameters from the focal mechanisms (Malagnini *et al.*, 2012). There is a very good agreement between the three sets of parameters. As discussed in the next two sections, for the linear inversion we used mostly the geological parameters to fix the geometrical constraints, while the rake angles where chosen in agreement with the focal mechanisms. In Figure S6 SUPPLEMENT we compare the fault plane obtained from the non linear inversions with the input fault geometry of the linear ones.

4.1 Deformation and modeling of the May 20th event

The May 20th event was modeled by inverting the CSK1 interferogram (Figure 3A), the RSAT-CSK2 difference map (Figure 3D and 4B), and the GPS data (Figure 3F). We constrained the model source to have a variable dip geometry, corresponding to the middle Ferrara thrust (Figure 1), with a shallower segment dipping at 40° followed at depth by a 20° sloping segment (Table 3). The modeled InSAR and GPS displacement fields and their residual values (observed minus modeled) are shown in Figure 3, whereas observed and modeled surface displacement profiles are shown in Figure 5.

Few GPS sites in the epicentral area recorded coseismic ground displacement from this earthquake (Figure 3): the MO05 site in Finale Emilia, moved ~3 cm to the SSW and uplifted ~7 cm; SGIP,

located South of the aftershock distribution, moved ~2 cm NNE; whereas SERM, located North of the aftershock distribution, moved southward of ~1.5 cm. The other sites showed planar displacements less than 1 cm in a radius of ~50 km from the epicenter (e.g., Bologna and Modena moved NNE-ward of ~7 mm). We measured reliable vertical displacements (~1 cm) only at SBPO, whereas for all other stations vertical displacements resulted below the noise level (Serpelloni *et al.*, 2012).

The RSAT-CSK2 deformation map consists of a main bulls-eye pattern, elongated WNW for ~25 km and ~10 km wide, with a maximum positive LOS displacement of ~21 cm (Figure 3D and 4B); a longitudinal profile (Figure 5A) shows a lower displacement gradient to the East, which may be attributed to the occurrence of two $M_L > 5$ aftershocks. To the West a smaller "whisker-shaped" deformation pattern is visible halfway between the displacement fields of the two main events (Figure 3D and 4B). This pattern show a central LOS maximum ground uplift of ~7 cm and two negative displacement areas to the North (~ -2 cm) and to the South (~ -3 cm, Figure 4B).

Since this pattern is not associated to any significant ($Ml \geq 5$) aftershock or foreshock of the May 20th event, it may represent displacement caused by slip on the May 20th fault plane, either as a coseismic rupture complexity or as a subsequent aseismic afterslip. In this case the position of the "whisker" pattern would imply that the slip occurred on the deeper part of the fault, below ~10 km depth. However, the observed displacement gradient (Figure 5B) is too steep to be reproduced by deep slip on the May 20th fault. In fact we verified that a joint inversion of all geodetic data up to May 27th (GPS, CSK1, RSAT-CSK2) generates high displacement residuals in the area of the "whisker-shaped" feature (Figure S7 SUPPLEMENT). Thus, this model does not explain the observed deformation satisfactorily.

The observed peculiar deformation pattern could also be explained with a complex faulting mechanism, with further slip occurring along an additional fault other than the Ferrara thrust, e.g. one of the shallower back thrust faults, a secondary splay of the main thrust fault or a different fault

altogether. Since the "whisker-shaped" deformation pattern is located directly above the Mirandola thrust front (Figure 1), we tested the possibility that the InSAR deformation shown in the RSAT-CSK2 map could be explained by inverting for slip occurred on both the Ferrara and Mirandola thrusts within the corresponding time span. Indeed, using this model we obtain a good fit to the data also in the “whisker-shaped” deformation area (Figure 5 A, B, C and D). Residual RMS values of 0.77 cm, 1.03 cm and 0.58 cm are observed with respect to the CSK1, RSAT-CSK2 and GPS data (Figure 3C and 3F). The slip distribution for this model shows a maximum slip of ~120 cm at 5 km depth on the NE fault (the Ferrara thrust), while the "whisker-shaped" displacement pattern is well modeled by slip (~30 cm) between 3 and 7 km depth on the SW fault plane (the Mirandola thrust, Figure 6A). The latter would correspond to a Mw >5 earthquake, which however is not observed in this area, suggesting that this is an aseismic slip event.

4.2 Deformation and modeling of the May 29th event

The InSAR displacement field of this Ml 5.8 earthquake (Figure 3G) is elongated ~E-W, with an extent of about 25 km and a maximum positive displacement of ~14 cm near the epicenter.

The horizontal GPS site displacements were all below 1 cm, since no stations were located in the near-field of the mainshock. All GPS planar vectors converge toward the area of highest InSAR displacement, with the exception of MO05, which shows movement toward SE (Figure 3I). We did not observe reliable patterns for the GPS vertical components, which were all below the noise level.

Following the same inversion scheme previously described, we linearly inverted the CSK2 displacement map (Figure 3G), and the GPS site displacements. These datasets span the ML 5.8 event and three aftershocks with ML >5 (Table 1 and Figure 1).

As for the May 20th event, we constrained the source location and geometry according to geological parameters (Table 3), and approximated the shape of the frontal Mirandola thrust by a shallower

segment dipping at 45° continuing at depth in a 30° dipping segment. The rake angle was fixed according to the focal mechanism (Malagnini *et al.*, 2012).

In this model we assume that the contribution of post-seismic deformation of the May 20th in this area is minimal, as verified from a further CSK ascending interferogram spanning the period May 22nd – May 26th (Figure S8 SUPPLEMENT).

The modeled slip distribution (Figure 6B) shows two main slip areas. In the central part of the fault a maximum slip of 54 cm is obtained at 6 km depth, corresponding to the main ground displacement pattern (Figure 3G). In the western side, a lower slip concentration (~30 cm) is located at slightly shallower depths (5 km). The relationships between these two slip areas is well depicted also in the E-W displacement profile (Figure 5F), and reflects the superposition of coseismic displacements from different sources. While the eastern displacement pattern can be correlated to the Ml 5.8 mainshock, the smaller displacement peak to the West cumulates the displacement due to the occurrence of three ML >5 aftershocks between May 29th and June 4th (Table 1 and Figure 1).

The modeled InSAR and GPS displacement fields and the residuals values are shown in Figures 3H and 3I, whereas the observed and modeled profiles of surface displacement are shown in Figure 5. A good fit is found between the observations and the model, with most residuals lying within ±2 cm and RMS values of 0.71 cm and 0.26 cm with respect to SAR and GPS observations. Near the town of Finale Emilia, high SAR (-4 cm) and GPS (Mo05 site, Figure 3I) residuals are observed, possibly related to local water table level readjustment and shallow fluid migration following the May 20th earthquake.

5. Stress readjustment

The distinctive features of the Emilia 2012 seismic sequence are the progressive Westward migration of the seismicity (Scognamiglio *et al.*, 2012) as well as the subsequent activation of close but distinct fault segments of similar size. In fact the May 29th event does not obey the characteristic seismicity rate decay predicted by the Omori law (see Scognamiglio *et al.*, 2012) and cannot be considered simply an aftershock of the May 20th mainshock. Such variations in the seismicity rate and spatial distribution during seismic sequences can often be attributed to static stress changes (Steacy *et al.*, 2005). We study the relationships between the largest earthquakes of the Emilia sequence by means of the Coulomb Failure Function (hereinafter ΔCFF, e. g. Harris, 1998).

Neglecting the contribution of the underground fluid pressure, Coulomb failure stress is defined as:

$$CFF= \tau+ \mu' \sigma-S$$

Where τ is the shear traction projected on the target fault plane, σ is the normal traction, defined positive for traction, μ' is the apparent friction coefficient that takes into account the pressure effects, and S is the rock cohesion, considered constant over time. Here μ' is kept fixed at a value of 0.4. The absolute stress values are often not known (Harris, 1998), and the Coulomb stress variation is computed. Since S at a first order approximation remains constant, the ΔCFF then becomes:

$$\Delta CFF= \Delta\tau+ \mu' \Delta\sigma$$

Positive ΔCFF due to stress readjustment following the mainshock, tends to advance subsequent shocks towards failure, while negative ΔCFF represents stress release and therefore a delayed fault failure-time.

To study the stress change induced by the May 20th mainshock on the May 29th fault plane, we project the six components of the stress tensor variation due to the former onto the slip direction of the latter. The ΔCFF shows an increase up to ~6 bar in the eastern sector of the May 29th fault,

(Figure 7) where we modeled aseismic slip responsible for the "whisker-shaped" deformation pattern.

In addition, we calculated the ΔCFF induced by both mainshocks on two receiver faults located W and NE of the seismic sequence, namely the western lateral ramp of the Mirandola thrust and the most external thrust of the Ferrara fold belt (Figures 1 and 7). For both faults, the stress variations are lower (~2.5 bar) than those computed on the May 29th fault plane but still not negligible with respect to the still debated minimum stress variation threshold magnitude (0.1 bar, e.g. Hardebeck *et al.* 1998).

6. Discussion and Conclusion

The Emilia seismic sequence filled a seismic gap existing at least since the year 1000 A.D. (Rovida *et al.*, 2011), and might therefore give important information on the mechanisms of strain accumulation and release in this area.

Regarding the long-term phase of strain accumulation, some considerations can be made based on our results. The InSAR data clearly show that the footprint of the coseismic deformation corresponds to part of the Mirandola and Ferrara folds, located at shallow depths under the Po alluvial plain. This evidence supports the long-term geomorphic analyses that attribute to the growth of the same folds the wide northward bend of the Po river course and the deviation of the Secchia and Panaro rivers (Burrato *et al.*, 2003). On the other hand no evident topographical bulge corresponds to the buried anticline crests (Figure 1), and this implies that the net fold growth rate must be lower than the sedimentation rate. In fact, for the Mirandola anticline, Scrocca *et al.* (2007) evaluate a relative tectonic uplift of 0.16 mm/yr in the last 125 ka, much lower than the estimated sedimentation rate (0.89 mm/yr) in the plain. Also GPS data confirm the absence of significant ongoing vertical deformation in this area (Bennett *et al.*, 2012; Devoti *et al.*, 2011).

One way to reconcile the interpretation of Burrato *et al*, 2003, with the absence of topographical relief in the area is to hypothesize that the repeated coseismic uplift events have progressively controlled the evolution of the hydrographic network.

For the Mirandola anticline, considering the 0.16 mm/yr long-term growth rate of the anticline crest, we calculate that about 800 year were needed to accumulate the crustal strain released during the 2012 coseismic displacement (~14 cm), This time lag is comparable with the duration of the quiescence in the seismic gap.

In the seismic hazard context, our modeling results demonstrate that the frontal blind thrusts below the Po plain are seismically active. The maximum magnitudes (Mw ~5.9) of the 2012 sequence are in agreement with those suggested by previous estimates (Valensise and Pantosti, 2001; DISS Working Group, 2010; Basili *et al*., 2008). Our results do not allow to consider this value as an upper bound, because, given the similar geometry and kinematics of the two main structures activated during the first 10 days of the sequence, their simultaneous rupture during a single event cannot be excluded (Hayes *et al.*, 2010). In this case an event with Mw > 6 could occur.

Moreover, the results of the stress transfer analysis, suggest that during the Emilia seismic sequence, the rupture of the Mirandola thrust (the May 29th event) was likely triggered by the additional stress load redistributed after the Ferrara thrust (the May 20th event). In this process, the aseismic slip occurred on the Mirandola thrust (modeled based on the "whisker" shaped deformation) may have played an important role. Although we cannot precisely place this slip event in time, it is reasonable to assume that it occurred in the time span between the two mainshocks, because: a) it is located in the portion of the Mirandola thrust more loaded by the May 20th shock, b) its main slip patches are spatially continuous with those modeled for the May 29th earthquake. Aseismic slip episodes related to earthquakes have been observed and modeled in terms of stress transfer in many seismotectonic contexts, either following (Fielding *et al.*, 2004) or preceding (Lohman and McGuire, 2007) earthquakes. Other analyses based on additional seismological data

might in the future further clarify the implications of stress transfer and earthquake triggering processes for the evaluation of time-dependent seismic hazard (Steacy *et al.*, 2005).

The 2012 Emilia seismic sequence represents an important reference point for the re-evaluation of the present tectonic activity of the Northern Apennine wedge, and provides useful new elements for the seismic hazard assessment. InSAR postseismic and long-term interseismic monitoring of crustal deformation will provide the necessary data for a better understanding of the strain accumulation and relaxation processes in this region.

Acknowledgements

The COSMO-SkyMed SAR data are copyright of ASI, and were provided by DPC in the framework of the ASI-INGV SIGRIS project. G.P. and J.P.M.B. were supported by ASI under the SIGRIS project contract. We thank all public and private institutions that manage and distribute the GPS data, in particular EUREF, ASI, IREALP, Regione Veneto and IGM. We thank FOGER for providing the Emilia-Romagna GNSS network, the Dept. of Earth Science of the University of Siena and the Dept. of Physics of the University of Bologna for providing data of the GPS station in Finale Emilia. We also thank GeoTop s.r.l. – Topcon-Sokkia Group and Leica Geosystems. Some figures were prepared using the public-domain GMT software (Wessel and Smith, 1998). We thank P. Burrato and L. Improta for the fruitful discussions and an anonymous reviewer for his useful comments.

References

Argnani, A., Bernini, M., Di Dio, G.M., Papani, G., Rogledi, S. (1997). Stratigraphic record of crustal-scale tectonics in the Quaternary of the Northern Apennines (Italy). *Il Quaternario* **10**(2): 595–602

Argnani, A., Barbacini, G., Bernini, M., Camurri, F., Ghielmi, M., Papani, G., Rizzini, F., Rogledi, S., Torelli, L. (2003). Gravity tectonics driven by Quaternary uplift in the Northern Apennines: insights from the La Spezia-Reggio Emilia geo-transect. *Quat Int,* **101**–102: 13–26

Atzori, S., I. Hunstad, M. Chini, S. Salvi, C. Tolomei, C. Bignami, S. Stramondo, E. Trasatti, A. Antonioli and E. Boschi (2009). Finite fault inversion of DInSAR coseismic displacement of the 2009 L'Aquila earthquake (Central Italy), *Geophys. Res. Lett.,* **36**, l15305, doi:10.1029/2009GL039293.

Atzori, S. and A. Antonioli (2011). Optimal fault resolution in geodetic inversion of coseismic data, *Geoph. J. Int*., **185**, 529-538, doi: 10.1111/j.1365-246X.2011.04955.x

Basili, R., G. Valensise, P. Vannoli, P. Burrato, U. Fracassi, S. Mariano, M.M. Tiberti, E. Boschi (2008). The Database of Individual Seismogenic Sources (DISS), version 3: summarizing 20 years of research on Italy's earthquake geology. *Tectonophysics*. **453**, 20-43. doi:10.1016/j.tecto.2007.04.014.

Bennett, R.A., E. Serpelloni, S. Hreinsdóttir, M.T. Brandon, G. Buble, T. Basic, G. Casale, A. Cavaliere, M. Anzidei, M. Marjonovic, G. Minelli, G. Molli and A. Montanari (2012). Syn-convergent extension observed using the RETREAT GPS network, northern Apennines, Italy, *J. Geophys. Res.,* **117**(B4), doi:10.1029/2011JB008744.

Bertotti, G., Capozzi, R. and Picotti, V. (1997). Extension controls Quaternary tectonics, geomorphology and sedimentation of the N-Apennines foothills and adjacent Po Plain (Italy). *Tectonophysics,* **282**: 291–301

Bigi, G., G. Bonardi, R. Catalano, D. Cosentino, F. Lentini, M. Parotto, R. Sartori, P. Scandone and E. Turco (Eds.) (1983). *Structural Model of Italy 1:500,000*. CNR Progetto Finalizzato Geodinamica.

Boccaletti, M., G. Corti and L. Martelli (2010). Recent and active tectonics of the external zone of the Northern Apennines (Italy). *Int J Earth Sci (Geol Rundsch)* **100**: 1331–1348, doi10.1007/s00531-010-0545-y.

Boccaletti, M. and L. Martelli (2004). (Coords): *Carta sismo-tettonica della Regione Emilia-Romagna scala 1:250.000 e note illustrative*, Selca, Firenze.

Burrato, P., F. Ciucci and G. Valensise (2003). An inventory of river anomalies in the Po Plain, Northern Italy: evidence for active blind thrust faulting. *Ann. of Geophys.* **46** (5), 865– 882.

Consiglio Nazionale delle Ricerche (1992). Structural Model of Italy and Gravity Map. Progetto Finalizzato Geodinamica. Quaderni de "*La Ricerca Scientifica*", **114**, Vol. 3

Devoti, R., A. Esposito, G. Pietrantonio, A.R. Pisani and F. Riguzzi (2011). Evidence of large scale deformation patterns from GPS data in the Italian subduction boundary, *Earth and Planetary Science Letters,* **311**(3-4), 1–12, doi:10.1016/j.epsl.2011.09.034.

Di Bucci, D. and Mazzoli, S. (2002). Active tectonics of the Northern Apennines and Adria geodynamics: new data and a discussion. *J Geodyn*, **34**: 687–707

DISS Working Group (2010). *Database of Individual Seismogenic Sources (DISS), Version 3.1.1*: A compilation of potential sources for earthquakes larger than M 5.5 in Italy and surrounding areas. http://diss.rm.ingv.it/diss/.

Emergeo Working Group: G. Alessio, L. Alfonsi, C. A. Brunori, P. Burrato, G. Casula, F. R. Cinti, R. Civico, L. Colini, L. Cucci, P. M. De Martini, E. Falcucci, F. Galadini, G. Gaudiosi, S. Gori, M. T. Mariucci, P. Montone, M. Moro, R. Nappi, A. Nardi, R. Nave, D. Pantosti, A. Patera, A. Pesci, G. Pezzo, M. Pignone, S. Pinzi, S. Pucci, S. Salvi, C. Tolomei, P. Vannoli, A. Venuti, and F. Villani (2013). Coseismic geological effects associated 1 with the Emilia 2 earthquake sequence of May-June 2012 (Northern Italy). *Nat. Hazards Earth Syst. Sci.*, **13**, 1–13.

Faccenna, C., Jolivet, L., Piromallo, C. and Morelli A. (2003). Subduction and the depth of convection in the Mediterranean mantle. *J Geophys Res.,* **108**(B2): 2099, doi:10.1029/2001JB001690

Farr, T. G., et al. (2007), The Shuttle Radar Topography Mission, Rev. Geophys., 45, RG2004, doi:10.1029/2005RG000183.

Fielding, E. J., T. J. Wright, J. Muller, B. Parsons, and R. Walker (2004). Aseismic deformation of a fold-and-thrust belt imaged by SAR interferometry near Shahdad, SE Iran *Geology*. **32**, 577–580.

Hayes G.P., Briggs R.W., Sladen A., Fielding E.J., Prentice C., Hudnut K., Mann P., Taylor W., Crone A.J., Gold R., Ito T., Simons M. (2010). Complex rupture during the 12 January 2010 Haiti earthquake. *Nature Geoscience* v. **3**, p. 800–805, doi:10.1038/ngeo977.

Hardebeck, J. L., J. J. Nazareth and E. Hauksson (1998). The static stress change triggering model: constraints from two southern California aftershock. *J. Geophys. Res.* **103**, 24427-24437.

Harris, R. (1998). Introduction to special section: Stress triggers, stress shadows, and implications for seismic hazard. *J. Geophys. Res.,* **103**, 24347-24358.

Levenberg, K. (1944). A Method for the Solution of Certain Non-Linear Problems in Least Squares. *The Quarterly of Applied Mathematics*. **2**, 164–168.

Lohman, R. B., and J. J. McGuire (2007). Earthquake swarms driven by aseismic creep in the Salton Trough, California. *J. Geophys. Res*., **112**, B04405, doi:10.1029/2006JB004596.

Malagnini, L., Hermann, R.B., Munafo' I., Buttinelli M., Anselmi M., Akinci A. and Boschi E. (2012). The 2012 Ferrara seismic sequence: regional crustal structure, earthquake sources, and seismic hazard, *Geophys. Res. Lett.* **39**, doi:10.1029/2012GL052314, in press.

Marquardt, D. (1963). An Algorithm for Least-Squares Estimation of Nonlinear Parameters. *SIAM J. on Applied Mathematics*. **11**, 431–441

Marzorati, S., Carannante, S., Cattaneo, M.,D'Alema, E., Frappicini, M., Ladina, C., Monachesi, G., Spallarossa, D. (2012). Automated control procedures and first results from the temporary

seismic monitoring of the 2012 Emilia sequence. *Annals of Geophys.*, **55**, 4, doi:10.4401/ag-6116

Meletti, C., Patacca, E. and Scandone, P. (2000). Construction of a Seismotectonic model: the case of Italy. *Pure Appl Geophys*, **157**: 11–35

Okada, Y. (1985). Surface deformation due to shear and tensile faults in a half-space. *Bull. Seismol. Soc. Am.*, **75**, 1135ñ1154.

Picotti, V. and F.J. Pazzaglia (2008). A new active tectonic model for the construction of the Northern Apennines mountain front near Bologna (Italy). J. *Geophys. Res.*, **113**, B08412, doi:10.1029/2007jb005307.

Pieri, M. (1983). Three seismic profiles through the Po Plain. In: Bally AW (ed) Seismic Expression of Structural Styles. A Picture and Work Atlas. Am. *Assoc. Pet. Geol. Studies in Geology*, 15: 3.4.1/8–3.4.1/26.

Pieri, M. and G. Groppi (1981). Subsurface geological structure of the Po plain, Italy: CNR, Progetto Finalizzato Geodinamica, 414, 13 p.

Rovida, A., R. Camassi, P. Gasperini and M. Stucchi (2011), (eds.). CPTI11, *the 2011 version of the Parametric Catalogue of Italian Earthquakes*. Milano, Bologna, http://emidius.mi.ingv.it/CPTI.

Salvi, S., C. Tolomei, J.P. Merryman Boncori, G. Pezzo, S. Atzori, A. Antonioli, E. Trasatti, R. Giuliani, S. Zoffoli and Coletta A., (2012). Activation of the SIGRIS monitoring system for ground deformation mapping during the Emilia 2012 seismic sequence, using COSMO-SkyMed InSAR data, *Ann. Geophys.*, **55**, 4, 2012; doi:10.4401/ag-6181.

Scognamiglio, L., L. Margheriti, F.M. Mele, E. Tinti, A. Bono, P. De Gori, V. Lauciani, F.P. Lucente, A.G. Mandiello, C. Marcocci, S. Mazza, S. Pintore and M. Quintiliani (2012). The 2012 Pianura Padana Emiliana seimic sequence: locations, moment tensors and magnitudes, *Annals of Geophysics*, **55** (4); doi:10.4401/ag-6159.

Scrocca, D., Carminati, E., Doglioni, C. and Marcantoni, D., (2007). Slab Retreat and Active Shortening along the Central-Northern Apennines. *Book Section: Thrust Belts and Foreland Basins Frontiers in Earth Sciences*, pp 471-487.

Serpelloni, E, Anderlini, L, Avallone, A., Cannelli, V., Cavaliere, A., Cheloni, D., D'Ambrosio, C, D'Anastasio, E., Esposito, A, Pietrantonio, G., Pisani, A.R., Anzidei, M., Cecere, G., D'Agostino, N., Del Mese, S., Devoti, R., Galvani, A., Massucci, A., Melini, D, Riguzzi, F., Selvaggi, G. and V. Sepe (2012). GPS observations of coseismic deformation following the May 20 and 29, 2012, Emilia seismic events (northern Italy): data, analysis and preliminary models, *Ann. Geophys.,* **55**, 4, 2012; doi: 10.4401/ag-6168

Serpelloni, E., M. Anzidei, P. Baldi, G. Casula and A. Galvani (2006). GPS measurement of active strains across the Apennines, *Ann. Geophys.,* **49** (1), 319–329.

Steacy, S., Gomberg, J., & Cocco, M. (2005). Introduction to special section: Stress dependent seismic hazard. *Journal of Geophysical Research*, **110**, B05S01, doi: 10.1029/2005JB003692.

Toscani, G., P. Burrato, D. Di Bucci, S. Seno and G. Valensise (2008). Plio-Quaternary tectonic evolution of the Northern Apennines thrust fronts (Bologna-Ferrara section, Italy): seismotectonic implications. *Boll. Soc. Geol. Ital.,* **128**, pp. 605–613.

Valensise, G. and Pantosti, D. (eds) (2001). Database of Potential Sources for Earthquakes Larger than 5.5 in Italy. *Ann Geof*, Suppl to vol. **44**(4), pp. 180, with CD-ROM, INGV

Wessel, P. and Smith, W.H.F. (1998). New, improved version of the generic mapping tools released. EOS, Transactions American Geophysical Union, **79**(47), pp. 579.

Table 1: Largest earthquakes (Ml>5) of the 2012 Emilia seismic sequence (http://iside.rm.ingv.it).

Origin Time (UTC)	**Ml**	**Latitude**	**Longitude**	**Depth (km)**
05/20/2012 02:03:52.000	5.9	44.89	11.23	6.3
05/20/2012 02:07:31.000	5.1	44.86	11.37	5.0
05/20/2012 13:18:02.000	5.1	44.83	11.49	4.7
05/29/2012 07:00:03.000	5.8	44.85	11.09	10.2
05/29/2012 10:55:57.000	5.3	44.89	11.01	6.8
05/29/2012 11:00:25.000	5.2	44.89	10.95	5.4
06/03/2012 19:20:43.000	5.1	44.90	10.94	9.2

Table 2: COSMO-SkyMed and Radarsat-1 SAR image pairs used for the study. The incidence angle is counted from the surface normal to the radar line-of-sight vector, whereas the heading angle is counted from North to the flight path direction. Values are referred to the center of the reference (master) geometry used for interferogram generation.

Name	Sensor	Orbit	Wavelength [cm] (Band)	Incidence angle [deg]	Heading angle [deg]	Acquisition dates	Perpendicular Baseline [m]
CSK1	COSMO-SkyMed	Desc.	3.12 (X)	29.22	168.85	May 19th May 23rd	365
CSK2	COSMO-SkyMed	Desc.	3.12 (X)	32.26	169.20	May 27th June 4th	425
RSAT	Radarsat-1	Desc.	5.66 (C)	34.47	170.84	May 12th June 5th	309

Table 3: Fault model parameters of the May 20th and May 29th sources.

Source		Length [km]	Width [km]	Top depth [km]	Strike [deg]	Dip [deg]	Rake [deg]	Maximum slip [cm]
May 20th source (middle Ferrara thrust)	Upper	34	11	1	114	40	90	120
	Lower		12	22.5		20		
May 29th source (frontal Mirandola thrust)	Upper	32	7.5	1	95	45	85	54
	Lower		10	12		30		

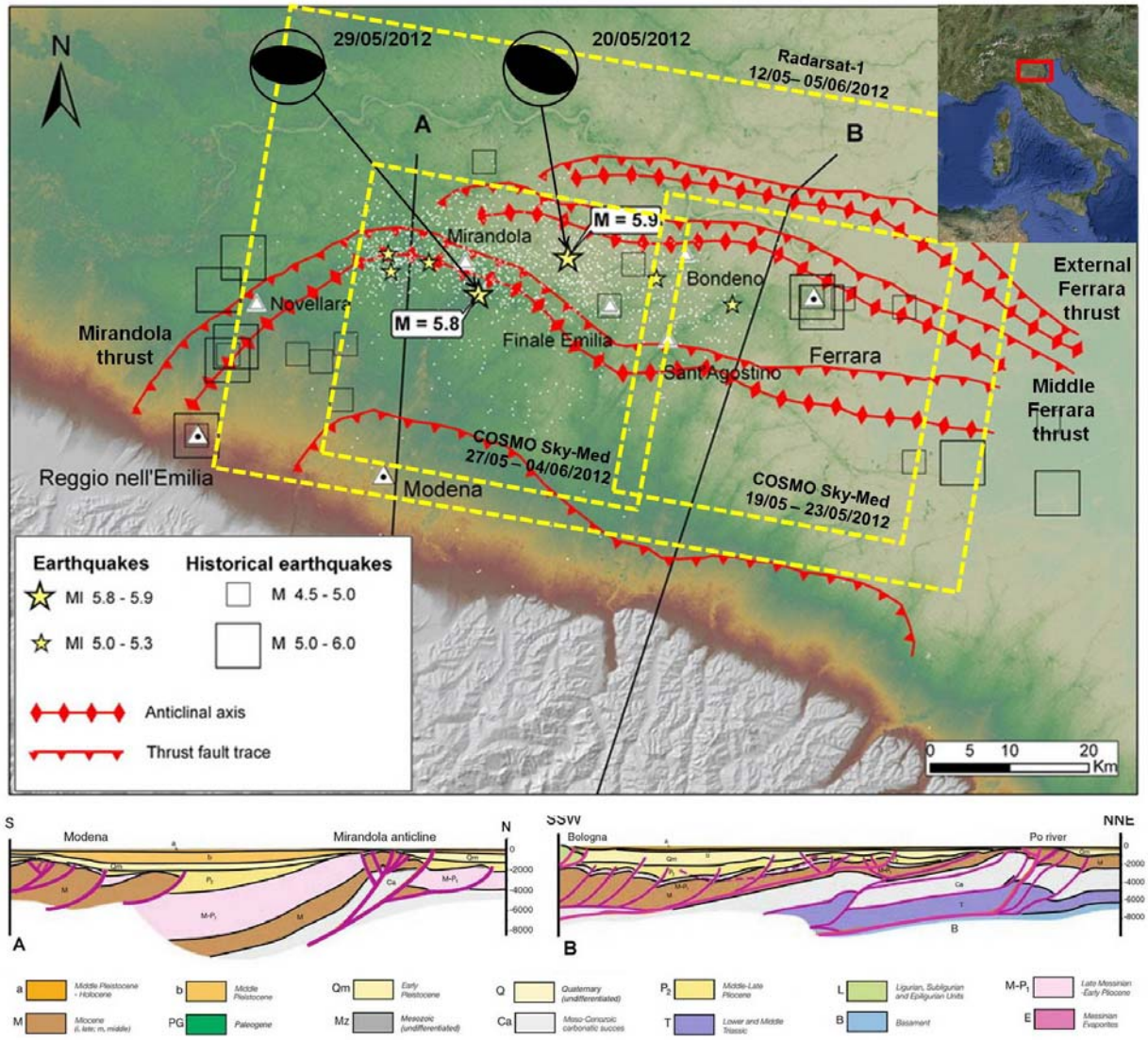

Figure 1: Top: Geo-structural setting of the Emilia 2012 seismic sequence area showing the vertically projected top traces of the main thrust fault planes, and the anticlinal axes, modified after (Boccaletti *et al.*, 2010; Picotti and Pazzaglia, 2012; Bigi *et al.*, 1983). White dots represent the aftershock epicenters. Large instrumental and historical earthquakes are also shown (http://iside.rm.ingv.it and Rovida *et al.*, 2011). Yellow rectangles indicate the footprint of the COSMO SkyMed (CSK) and Radarsat satellite image pairs. The focal mechanisms of the two main events (from Malagnini *et al.*, 2012) are reported in the map. Bottom: Geological profiles interpreted from seismic reflection data after (Boccaletti *et al.*, 2010) corresponding to traces A and B in the top panel.

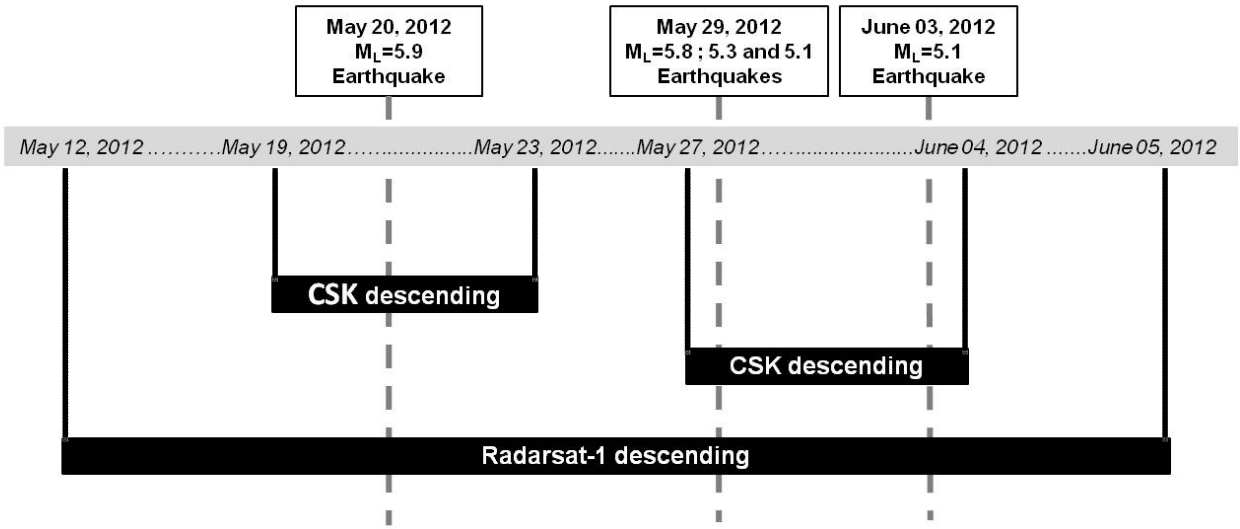

Figure 2: Graphical illustration of the temporal relationship between the three SAR image pairs used in this study and the main earthquakes (M_L > 5.0) of the Emilia seismic sequence.

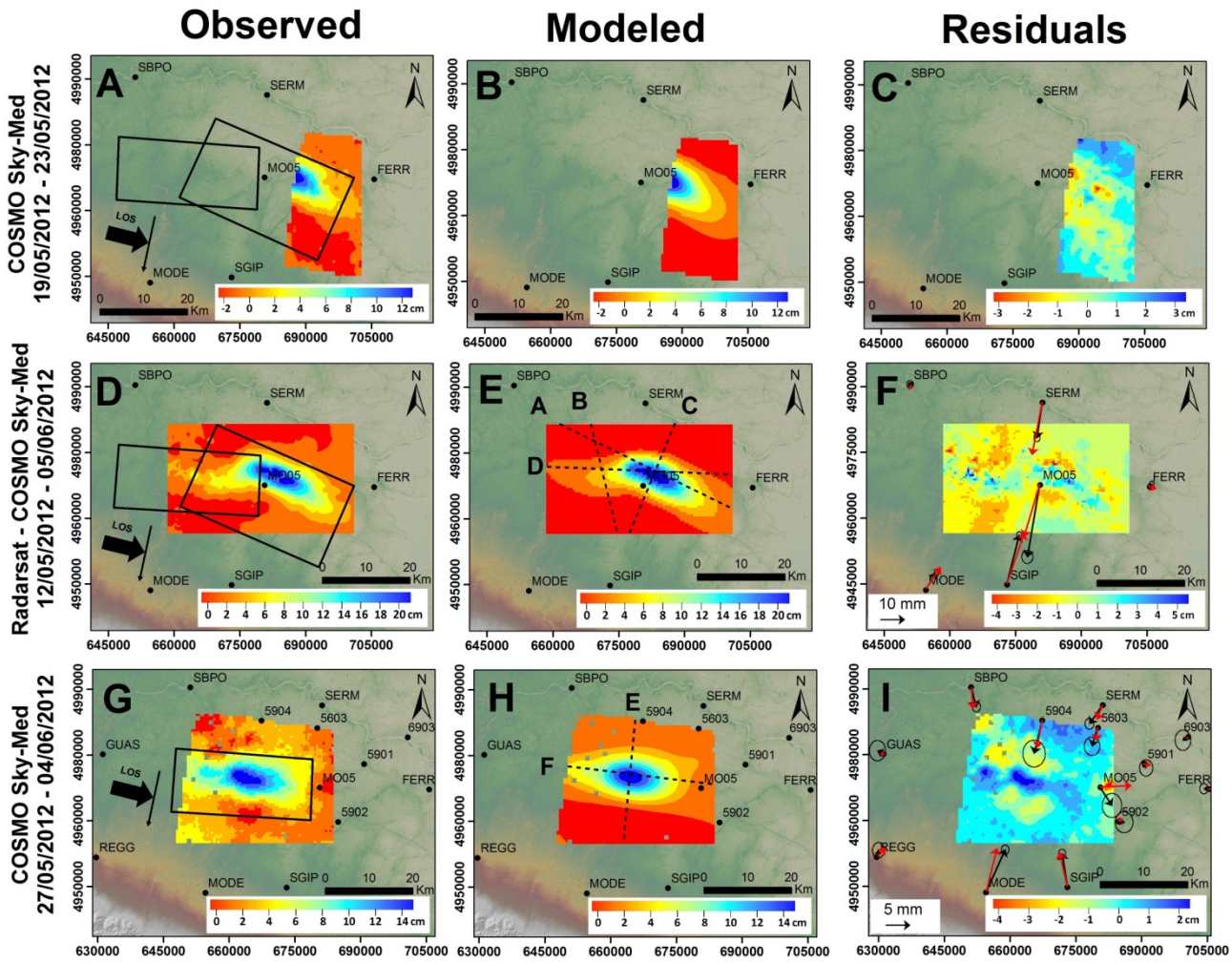

Figure 3: (left) Observed, (middle) modeled, and (right) residual displacement maps of two unwrapped COSMO-SkyMed interferograms and one Radarsat *minus* COSMO-SkyMed (as specified in the main text) map relating to the May 20th (panels from A to F) and May 29th (panels from G to I) earthquakes. Satellite paths and line of sight (LOS) directions are shown in panels A, D and G. Data set details are supplied in Table 2. Black boxes indicate the surface projections of the modeled faults. Black dashed lines indicate the traces of the profiles shown in Figure 5. In panels F and I we show the GPS modeled (red) and observed (black) displacements for the May 20th and 29th events, respectively.

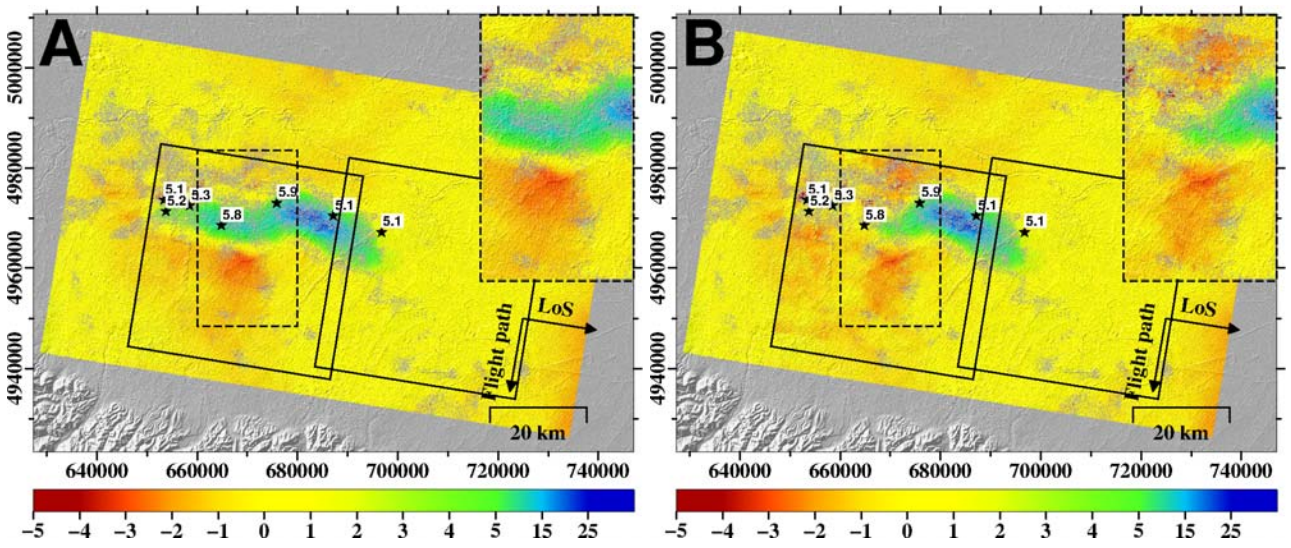

Figure 4: (A) Cumulative displacement map spanning all main events of the sequence, obtained from the Radarsat-1 May 12th - June 5 th interferogram (B) Cumulative displacement between May 12th and May 27th and June 4th to June 5 th, obtained by subtracting the COSMO-SkyMed May 27th - June 4th displacement from the map shown in panel A. Solid-line black rectangles indicate the footprint of the COSMO SkyMed satellite image pairs. The insets in the top-right corners contain a zoom of the area enclosed by the dashed-line black rectangles. Arrows indicate the ground-projected line-of-sight (from ground to satellite) and the satellite flight path. The inset in panel B shows the "whisker" shaped deformation mentioned in the text.

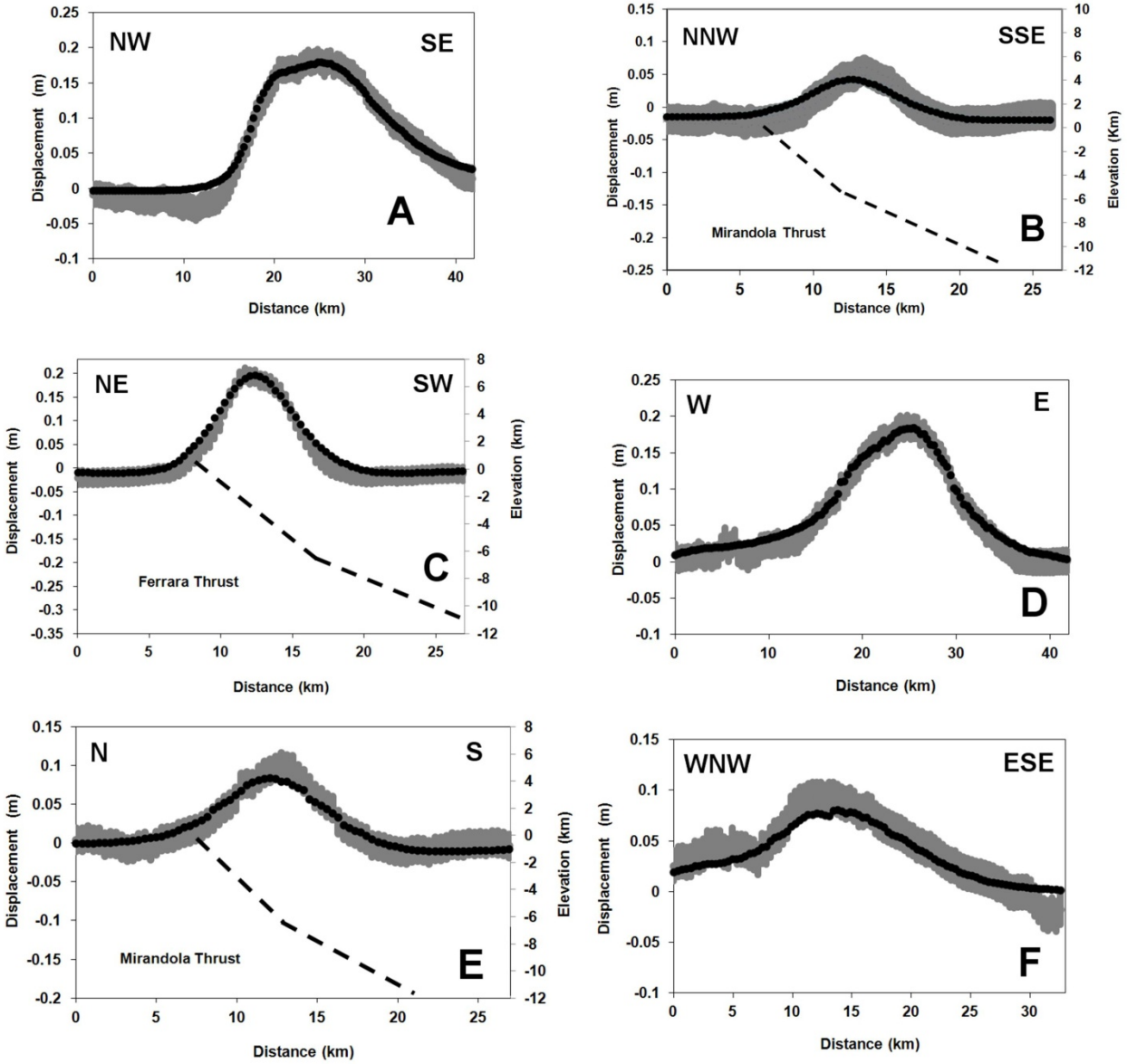

Figure 5: Observed (gray), and modeled (black) displacement profiles for the May 20th (from A to D) and May 29th (E and F) seismic events. A mean error bar of 1.5 cm is associated to the SAR-data. Black dashed lines illustrate the modeled fault traces. The profile traces are shown in Figure 3.

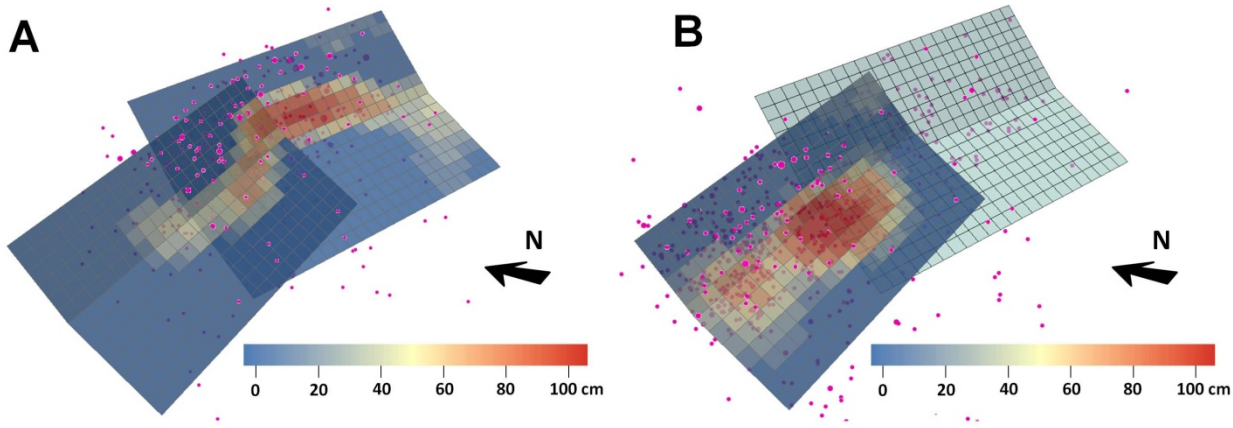

Figure 6: Panels A and B show the slip distribution (1.5 x 1.5 km patches) along the May 20th and May 29th sources respectively. Purple spheres represent the hypocenter (http://iside.rm.ingv.it) (M_L > 2) relative to the following time spans: May 17th – May 28th 2012 (panel A) and May 29th – June 11th 2012 (panel B).

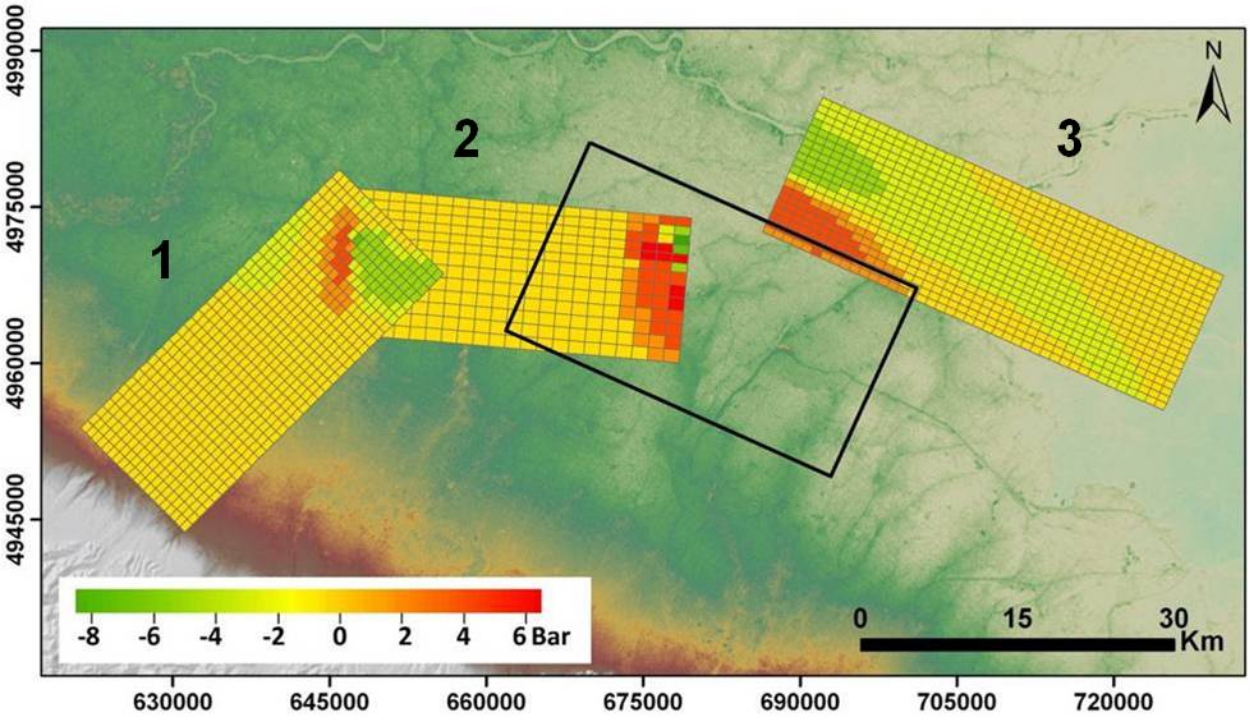

Figure 7: Results of the CFF analysis for three different fault planes. The source of the May 20th seismic event, outlined in black, was used to calculate the Coulomb stress changes on the May 29th plane (fault B). The patch size is 1.5 x 1.5 km. Both May 20th and May 29th faults were used to calculate the ΔCFF on the western lateral ramp of the Mirandola thrust (fault A), defined according to geological data (Boccaletti *et al.*, 2010), and on the external thrust of the Ferrara fold belt (fault C, Boccaletti *et al.*, 2010). For faults A and C the patch size is 1 x 1 km. See also Figure 1 for thrust locations.